第 33 卷第 4 期
2017 年 4 月

无 机 化 学 学 报
CHINESE JOURNAL OF INORGANIC CHEMISTRY

Vol.33 No.4
664-672

# 两种固体荧光有机–无机杂化物的合成、结构及强红光发射

田 悦[1] 李 飞*,[1] 张国翠[1] 周虹屏[1] 吴杰颖[1] 田玉鹏[1,2]

([1]安徽大学无机功能材料化学重点实验室,合肥 230601)

([2]南京大学配位化学重点实验室,南京 210093)

**摘要**:采用(*E*)-4-(4-(diphenylamino)styryl)-1-methylpyridinium iodide(DPASPI,DPASP=(*E*)-4-(4-(diphenylamino)styryl)-1-methylpyridinium),设计合成 2 种新型有机–无机杂化物(DPASP)$_2$[Zn(NCS)$_4$]·2CH$_3$OH (**1**)和{(DPASP)$_2$[Cd(SCN)(NCS)$_3$]·2CH$_3$OH}$_n$ (**2**)。通过单晶 X 射线衍射进行了表征,结果表明杂化物 **1** 和 **2** 是由有机吡啶阳离子和异硫氰酸金属配阴离子组成的,具有不同空间结构。通过 $^1$H NMR 谱图解释了离子间相互作用。对具有高量子产率的杂化物 **1** 和 **2** 的红光发光性质进行了研究。

**关键词**:有机–无机杂化物;大量高效合成;晶体结构;红光发射性质

**中图分类号**:O614.24$^+$1;O614.24$^+$2 **文献标识码**:A **文章编号**:1001-4861(2017)04-0664-09

**DOI**:10.11862/CJIC.2017.060

## Two Solid Fluorescent Organic-Inorganic Hybrids: Synthesis, Crystal Structures and Strong Red Fluorescence Emissions

TIAN Yue[1] LI Fei*,[1] ZHANG Guo-Cui[1] ZHOU Hong-Ping[1] WU Jie-Ying[1] TIAN Yu-Peng[1,2]

([1]*Department of Chemistry, Key Laboratory of Functional Inorganic Materials Chemistry of Anhui Province, Anhui University, Hefei* 230601, *China*)

([2]*State Key Laboratory of Coordination Chemistry, Nanjing University, Nanjing* 210023, *China*)

**Abstract:** Two organic-inorganic hybrids, (DPASP)$_2$[Zn(NCS)$_4$]·2CH$_3$OH (**1**) and {(DPASP)$_2$[Cd(SCN)(NCS)$_3$]·2CH$_3$OH}$_n$ (**2**), have been facilely prepared from (*E*)-4-(4-(diphenylamino)styryl)-1-methylpyridinium iodide(DPASPI, DPASP =(*E*)-4-(4-(diphenylamino)styryl)-1-methylpyridinium) at gram scale. Their crystal structures have been confirmed by single-crystal X-ray diffraction analysis, which show that the hybrids **1** and **2** consist of organic pyridium cations and metal thiocyanato anions bearing different spacial structure through self-assembly processes. Furthermore, the interactions between the ions have been investigated by $^1$H NMR spectra. Finally, red photolumencent properties with enhanced quantum yields of hybrids **1** and **2** were investigated. CCDC: 1517533, **1**; 1060372, **2**.

**Keywords:** organic-inorganic hybrid; scalable efficient synthesis; crystal structure; red photoluminescent property

## 0 Introduction

Recently, organic-inorganic hybrid materials have attracted considerable interest due to their potential application in nanomedicine, catalysis and photoactive devices[1-3]. One important hybrid, pyridinium salt, has also been focused on. Researchers have taken much effort to design and synthesize novel pyridinium salts with the push-pull $\pi$-conjugated dipolar feature in the pursuit of enhancing the intramolecular charge

收稿日期:2016-09-01。收修改稿日期:2016-12-26。

国家自然科学基金(No.51372003,51432001,51472002,51672002)资助项目。

*通信联系人。E-mail:lfe@ahu.edu.cn

transfer (ICT) upon excitation[4-5]. Multiple pyridinium salts containing porphyrin[6-7], carbazole[8], tetraphenylethene[9-10] and triphenylamine unit[11], are designed for photolumincent organic-inorganic hybrid materials on plentiful photoluminescent applications, including second harmonic generation imaging, dye-sensitized solar cells (DSSCs), DNA photocleavage and chemosensor. In general, the bulk of pyridinium salts assemble with anions, such as $I^-$, $Br^-$, $BF_4^-$, $PF_6^-$[12-13].

The thiocyanato anion, as a versatile ligand, plays a functional role in cooperative magnetic properties on the applications of coordination polymers (CPs) or metal-organic frameworks (MOFs), owing to adopting multiple coordination modes[14]. There are different styles of the coordination networks varying from the metals and ligands[15]. In addition, as having $d^{10}$ electronic configuration, the metal ions $Zn^{2+}$ and $Cd^{2+}$ are particular flexible for the construction of coordination networks varying from tetrahedral to octahedral; are reversible for the formation of coordination bonds enabling to rearrange metal ions and ligands in highly regular networks; are feasible to all kinds of architectures and the topological types, which have attracted extensive attention upon optical, electronic and magnetic properties[16]. Our previous work, Tian et al.[17] have successfully synthesized a series of *trans*-4-(4′-*N*,*N*-dialkylaminostyryl)-*N*-methyl pyridinium and its derivatives featuring with $[Cd(SCN)_3]_n^-$ and applied them in nonlinear optical materials. So far, the zig-zag of $[M(NCS)_n]$ chains through thiocy-anato bridge as metal anions have diversified the architectural beauty of coordination hybrids, taking advantages as mentioned above[18]. Therefore, it is highlight that organic-inorganic hybrid materials achieve peculiar and induced photoluminescent properties via easy synthesis, well-defined structure and molecular arrangement.

In this work, two organic-inorganic hybrid materials $(DPASP)_2[Zn(NCS)_4]\cdot 2CH_3OH$ (**1**) and $\{(DPASP)_2[Cd(SCN)(NCS)_3]\cdot 2CH_3OH\}_n$ (**2**) have been synthesized from (*E*)-4-(4-(diphenylamino)styryl)-1-methylpyridinium iodide(DPASPI). They have been characterized by $^1$H NMR, $^{13}$C NMR, and FT-IR spectra, then structurally characterized by single-crystal X-ray diffraction analysis. Their structure-property relationships have been preliminarily investigated. For the first time, two pyridinium salts with strong red fluorescence emissions have been investigated.

## 1 Experimental

### 1.1 Materials and general procedures

All of the chemicals and solvents were purchased from commercially available resources with further purification by conventional methods. The $^1$H NMR and $^{13}$C NMR spectra were recorded at 25 ℃ using Bruker Avance 400 spectrometer with TMS as internal standard. FT-IR spectra were recorded on NEXUS 870 (Nicolet) spectrophotometer in the 400~4 000 $cm^{-1}$ region using a powder sample on a KBr plate. The solid-state luminescence spectra were measured on an F-4500 FL spectrophotometer with the EX Slit: 5.0 nm, EM Slit: 5.0 nm, and PMT Voltage: 700 V for DPASPI, hybrids **1** and **2**. For time-resolved fluorescence measurements, the fluorescence signals were collimated and focused onto the entrance slit of a monochromator with the output plane equipped with a photomultiplier tube (HORIBA HuoroMax-4P). The decays were analyzed by least-squares. The quality of the exponential fits was evaluated by the goodness of fit ($\chi^2$). Quantum yield was measured by integrating sphere. Thermogravimetry (TG) and differential thermogravimetry (DTG) methods in the temperation range from 50 to 800 ℃ under a flowing atmosphere of nitrogen.

### 1.2 Synthesis of the hybrids

#### 1.2.1 Synthesis of DPASPI

DPASPI was prepared according to the literature method[17,19]. $^1$H NMR (DMSO-$d_6$, 400 MHz): $\delta$ 8.792 (d, *J*=6.8 Hz, 2H), 8.155 (d, *J*=6.8 Hz, 2H), 7.955 (d, *J*=16.4 Hz, 1H), 7.629 (d, *J*=8.8 Hz, 2H), 7.370 (t, *J*=7.8 Hz, 4H), 7.316 (d, *J*=16.4 Hz, 1H), 7.153 (t, *J*=7.4 Hz, 2H), 7.104 (d, *J*=8.0 Hz, 4H), 6.931 (d, *J*=8.8 Hz, 2H), 4.225 (s, 3H); $^{13}$C NMR (DMSO-$d_6$, 100 MHz): $\delta$ 152.780, 149.385, 146.170, 144.749, 140.450, 129.829, 129.662, 127.987, 125.354, 124.464, 122.888, 120.672, 120.443, 46.700. FT-IR (KBr, $cm^{-1}$): 3 435 (w), 1 578

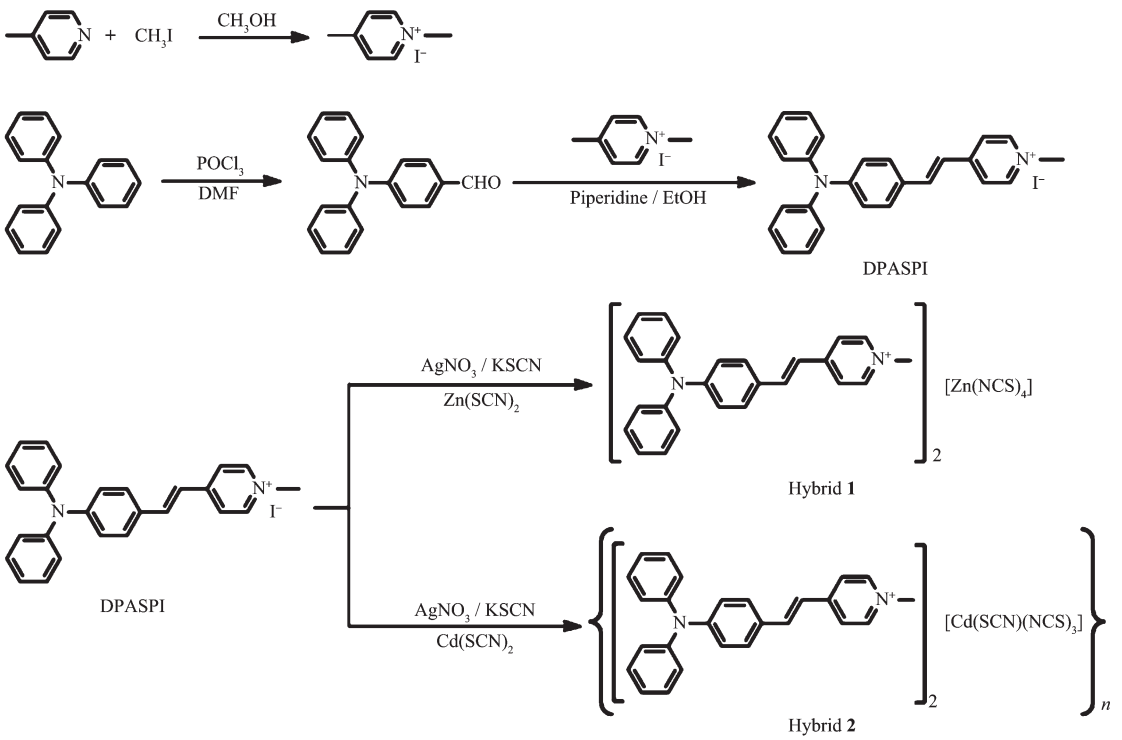


Scheme 1 Synthesis routes for hybrids **1** and **2**

(vs), 1 515 (vs), 1 487 (vs), 1 329 (s), 1 283 (s), 1 178 (vs), 978 (w), 836 (m), 754 (m), 695 (m), 536 (m).

1.2.2 Synthesis of **1**

$AgNO_3$ (1.70 g, 10 mmol) in 20 mL methanol was added to 30 mL methanol solution of DPASPI (4.90 g, 10 mmol). The mixture was refluxed for 3 h, and then filtered to remove silver iodide precipitation. The filtrate was added into 20 mL methanol solution of KSCN (0.97 g, 10 mmol), followed by refluxing for about 3 h and then filtered to remove $KNO_3$. After evaporation of the clear red solution, shining micro-crystals were formed, filtered, washed with water and methanol, and pure product A was obtained. Pure product A (1.27 g, 3.00 mmol) and $Zn(SCN)_2$ (0.55 g, 3.00 mmol) were refluxed in 25 mL methanol. Red product was obtained by filtration. Yield: 1.60 g, 81%. $^1$H NMR (DMSO-$d_6$, 400 MHz): $\delta$ 8.768 (d, $J$=6.4 Hz, 2H), 8.131 (d, $J$=6.4 Hz, 2H), 7.930 (d, $J$=16.0 Hz, 1H), 7.620 (d, $J$=8.8 Hz, 2H), 7.381 (t, $J$=7.8 Hz, 4H), 7.290 (d, $J$=16.0 Hz, 1H), 7.164 (t, $J$=7.4 Hz, 2H), 7.120 (d, $J$=7.6 Hz, 4H), 6.950 (d, $J$=8.4 Hz, 2H), 4.251 (s, 3H); $^{13}$C NMR (DMSO-$d_6$, 100 MHz): $\delta$ 152.798, 149.433, 146.180, 144.752, 140.490, 133.387, 129.814, 129.622, 127.950, 125.367, 122.885, 120.692, 120.442, 46.646. FT-IR (KBr, cm$^{-1}$): 3 032 (w), 2 363 (w), 2 071 (vs), 1 579 (vs), 1 519 (vs), 1 489 (vs), 1 329 (s), 1 292 (s), 1 172 (vs), 692 (w), 667 (w), 534 (m) (Fig.4). Anal. Calcd. for $C_{36}H_{31}N_{10}O_2S_8Zn_2$(%): C, 42.27; H, 3.05; N, 13.69. Found(%): C, 42.78; H, 3.01; N, 14.09.

1.2.3 Synthesis of **2**

The synthesis of **2** was same with hybrid **1** except that $Zn(SCN)_2$ was changed into $Cd(SCN)_2$ (0.68 g, 3.00 mmol). Color: red. Yield: 1.94 g, 92%. $^1$H NMR (DMSO-$d_6$, 400 MHz): $\delta$ 8.773 (d, $J$=6.4 Hz, 2H), 8.129 (d, $J$=6.4 Hz, 2H), 7.922 (d, $J$=16.4 Hz, 1H), 7.613 (d, $J$=8.8 Hz, 2H), 7.362 (t, $J$=7.8 Hz, 4H), 7.285 (d, $J$=16.4 Hz, 1H), 7.146 (t, $J$=7.4 Hz, 2H), 7.092 (d, $J$=7.6 Hz, 4H), 6.925 (d, $J$=8.8 Hz, 2H), 4.222 (s, 3H); $^{13}$C NMR (DMSO-$d_6$, 100 MHz): $\delta$ 152.797, 149.407, 146.194, 144.776, 140.484, 129.824, 129.660, 128.012, 125.358, 124.468, 122.922, 120.709, 120.492, 46.663. FT-IR (KBr, cm$^{-1}$): 3 032 (w), 2 359 (w), 2 077 (vs), 1 580 (vs), 1 516 (vs), 1 488 (vs), 1 333 (s), 1 287 (s), 1 208 (s), 1 171 (vs), 976 (w), 835 (w), 756 (m), 696 (m), 536 (m) (Fig.4). Anal. Calcd. for $C_{32}H_{31}CdN_6O_2S_4$(%): C, 49.77;

H, 4.05; N, 10.88. Found(%): C, 49.06; H, 4.23; N, 11.08.

### 1.3 Single-crystal X-ray diffraction analysis

The X-ray diffraction measurements were perfo-rmed on a Bruker SMART CCD area detector using graphite monochromated Mo $K\alpha$ radiation ($\lambda$=0.071 069 nm) at 296 K. Intensity data were collected in the variable $\omega$-scan mode. The structures were solved by direct methods and difference Fourier syntheses. The non-hydrogen atoms were refined anisotropically and hydrogen atoms were introduced geometrically. Calculations were performed with the SHELXTL-97 program package[20]. The crystal data and structure refinement parameters were listed in Table 1.

CCDC: 1517533, **1**; 1060372, **2**.

**Table 1　Crystal data and structure refinement parameters for hybrids 1 and 2**

| | 1 | 2 |
|---|---|---|
| Empirical formula | $C_{116}H_{108}N_{16}O_4S_8Zn_2$ | $C_{58}H_{54}N_8O_2S_4Cd$ |
| Formula weight | 2 177.40 | 1 135.73 |
| Crystal system | Triclinic | Triclinic |
| Space group | $P\bar{1}$ | $P\bar{1}$ |
| $a$ / nm | 0.998 8(7) | 0.903 9(12) |
| $b$ / nm | 1.048 8(8) | 1.140 4(15) |
| $c$ / nm | 2.794(2) | 2.761 8(4) |
| $\alpha$ / (°) | 83.124(9) | 100.756(2) |
| $\beta$ / (°) | 84.313(9) | 92.295(2) |
| $\gamma$ / (°) | 74.843(10) | 102.265(2) |
| $V$ / nm$^3$ | 2.798(4) | 2.723 5(6) |
| $Z$ | 1 | 2 |
| $D_c$ / (Mg·m$^{-3}$) | 1.292 | 1.385 |
| Absorption coefficient / mm$^{-1}$ | 0.64 | 0.604 |
| $F$(000) | 1 136 | 1 172 |
| $\theta$ range / (°) | 2.2~24.0 | 0.8~25.5 |
| $R_{int}$ | 0.050 | 0.028 |
| $R$ indices (all data) | $R_1$=0.080 1, $wR_2$=0.242 4 | $R_1$=0.065 8, $wR_2$=0.200 6 |
| Goodness of fit | 1.07 | 1.06 |

## 2 Results and discussion

### 2.1 Structural description of hybrids 1 and 2

Hybrid **1** crystallizes in the triclinic $P\bar{1}$ space group. The asymmetric unit contains one $[Zn(NCS)_4]^{2-}$ anion, two DPASP cations and two $CH_3OH$ molecules. $Zn^{2+}$ ion is four-coordinated by four nitrogen atoms of four distinct $NCS^-$ anions (Fig.1a). As listed in Table 2, the Zn-N bond lengths fall between 0.193 9(7) and 0.198 1(8) nm, and the angles of N-Zn-N range from 106.22(3)° to 114.13(3)°. As shown in Fig.1b, the molecules of **1** are connected by DPASP cations forming hydrogen bonding interactions with the S atom of $[Zn(NCS)_4]^{2-}$ anions (C27-H27B…S2 0.283 2(4) nm), and C20-H20…$\pi$ (0.371 7(2) nm) and C43-H43…$\pi$ (0.354 5(2) nm) contacts. As Zn…Zn…Zn angle is 180°, the $[Zn(NCS)_4]^{2-}$ anions and DPASP cations are parallel to one another and run along the crystallographic $a$ axis. As shown in Fig.1c, the hydrogen bond (C2-H2…S1 0.273 9(2) nm) and C46-H46…$\pi$ (0.273 9(2) nm) interactions between adjacent layers assemble neighboring wavelike layers to form highly regular 2D network. Therefore, the alleged 2D network is constructed from the connection between $[Zn(NCS)_4]^{2-}$ anion and DPASP cations through hydrogen bonding interactions in hybrid **1**.

Compared to hybrid **1**, anions in hybrid **2** as bridging ligands play an important role in the coordination polymers, as well as terminal groups[21]. Hybrid **2** also crystallizes in the triclinic $P\bar{1}$ space group. The

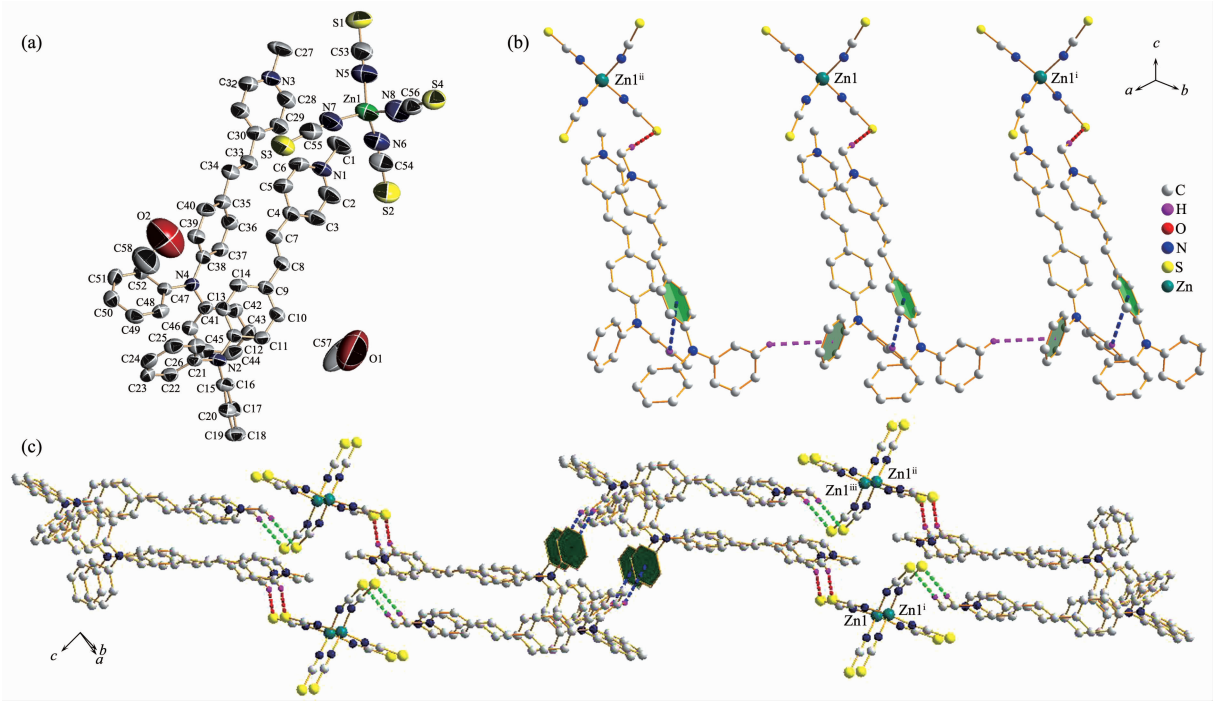


Thermal ellipsoids are drawn at the 50% probability level for (a); Symmetry codes: [i] $x-1, y+1, z$; [ii] $x+1, y-1, z$ in (b); [i] $x-1, y+1, z$; [ii] $-x-1, 1-y, 1-z$; [iii] $-x, -y, 1-z$ in (c)

Fig.1 (a) ORTEP diagram of hybrid **1**; (b) 1D chain bridged by C–H···S and C–H···$\pi$ in hybrid **1**; (c) 2D layer formed by C–H···S and C–H···$\pi$ in hybrid **1**

**Table 2 Selected bond lengths (nm) and bond angles (°)**

| | | | | | |
|---|---|---|---|---|---|
| Hybrid **1** | | | | | |
| Zn(1)-N(5) | 0.197 9(6) | Zn(1)-N(7) | 0.193 9(7) | O(1)-C(57) | 0.143 2(9) |
| Zn(1)-N(6) | 0.196 5(7) | Zn(1)-N(8) | 0.198 2(8) | O(2)-C(58) | 0.143 0(8) |
| N(5)-Zn(1)-N(6) | 114.13(3) | N(5)-Zn(1)-N(8) | 106.22(3) | N(6)-Zn(1)-N(8) | 107.74(3) |
| N(5)-Zn(1)-N(7) | 109.28(3) | N(5)-Zn(1)-N(7) | 109.33(3) | N(7)-Zn(1)-N(8) | 110.06(3) |
| Hybrid **2** | | | | | |
| Cd(1)-N(7) | 0.224 7(6) | Cd(1)-S(1) | 0.264 79(17) | S(2)-Cd(1)[ii] | 0.276 82(15) |
| Cd(1)-N(8) | 0.231 1(5) | Cd(1)-S(4)[i] | 0.274 17(14) | S(4)-Cd(1)[ii] | 0.274 17(14) |
| Cd(1)-N(6) | 0.235 0(5) | Cd(1)-S(2)[ii] | 0.276 82(15) | | |
| N(6)-Cd(1)-S(1) | 83.79(2) | N(6)-Cd(1)-S(4)[i] | 87.04(2) | S(1)-Cd(1)-S(4)[i] | 87.35(5) |
| N(7)-Cd(1)-N(6) | 91.5(2) | N(7)-Cd(1)-S(4)[i] | 94.56(2) | S(1)-Cd(1)-S(2)[ii] | 91.15(5) |
| N(7)-Cd(1)-S(1) | 174.79(2) | N(8)-Cd(1)-S(4)[i] | 92.68(2) | | |

Symmetry codes: [i] $x, y+1, z$; [ii] $-x+2, -y+1, -z+1$

asymmetric unit include one $[Cd(SCN)(NCS)_3]^{2-}$ anion, two DPASP cations and two $CH_3OH$ molecules. In comparison with hybrid 1, $Cd^{2+}$ ion is four-coordinated to three nitrogen atoms and one sulfur atom (Fig.2a). The Cd-N distances are 0.224 7(6), 0.231 1(5) and 0.235 0(5) nm, respectively, and Cd-S distance is 0.264 8(17) nm; the bond angles around Cd are in the range of 83.79(2)°~174.79(2)° (Table 2). In hybrid **2**, the 1D linear framework is constructed by linear $\{[Cd(SCN)(NCS)_3]^{2-}\}_n$ chains together via a series of weak intra- and inter-chain C–H···S (C50–H50···S3 0.299 4(3) nm, C51–H51···S1 0.291 4(2) nm and

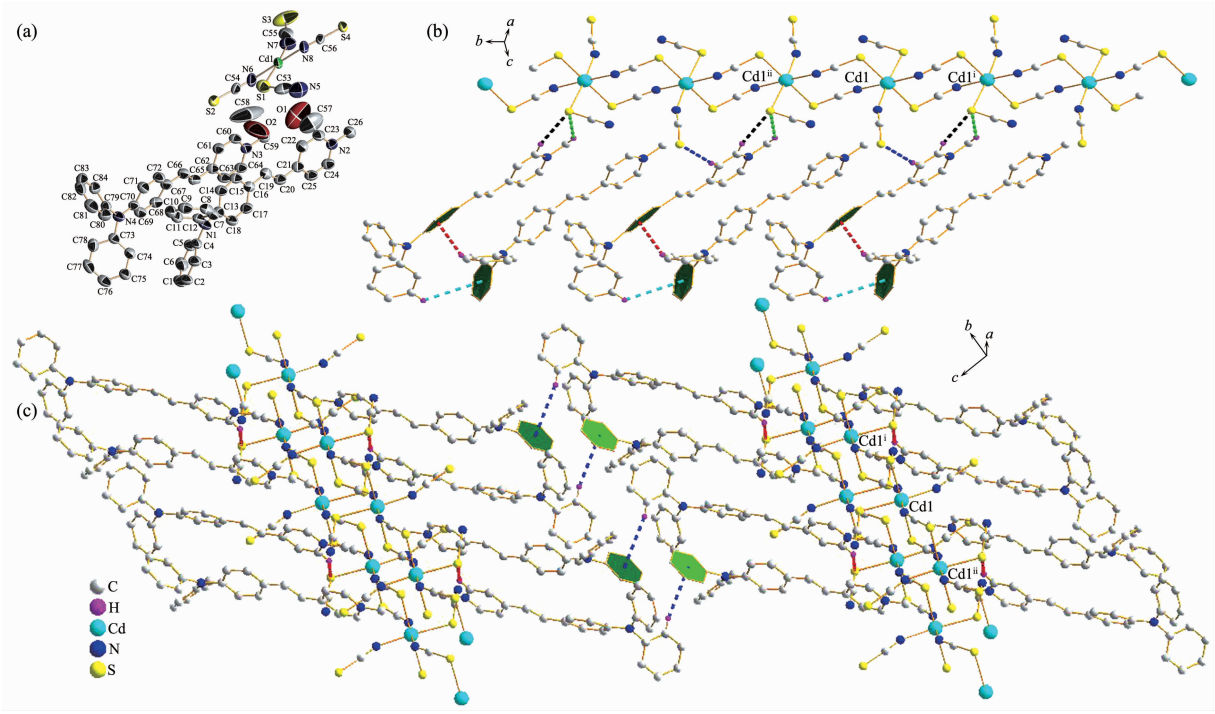


Thermal ellipsoids are drawn at the 50% probability level for (a); Symmetry codes: [i] 2–*x*, 1–*y*, 1–*z*; [ii] 2–*x*, –*y*, 1–*z* in (b); [i] 2–*x*, 1–*y*, 1–*z*; [ii] 2–*x*, –*y*, 1–*z* in (c)

Fig.2　(a) ORTEP diagram of hybrid **2**; (b) 1D chain bridged by C–H···S and C–H···$\pi$ in hybrid **2**; (c) 2D layer formed by C–H···S and C–H···$\pi$ in hybrid **2**

C52–H52B···S1 0.298 8(2) nm) and C–H···$\pi$ (C11–H11···$\pi$ 0.303 7(4) nm and C29–H29···$\pi$ 0.358 9(4) nm) interactions (Fig.2b). Adjacent $Cd^{2+}$ ions are linked by two bridging thiocyanato anions with the Cd···Cd distances of 0.566 6(9) and 0.577 5(9) nm, which are shorter than the average distance of two adjacent Zn distance (*ca.* 0.998 8(8) nm) in hybrid **1**, and Cd···Cd···Cd angle is 170.84(9)°. As displayed in Fig.2c, the 1D $\{[Cd(SCN)(NCS)_3]^{2-}\}_n$ chains can be further extended to a 2D supramolecular structure through the weak interactions (C47–H47···S1 0.287 9(2) nm and C33–H33···$\pi$ 0.337 7(3) nm) with DPASP cations as counterions forming 2D layer of hybrid **2**.

### 2.2　$^1$H NMR and FT-IR spectra of DPASPI, hybrids 1 and 2

Furthermore, the interactions can also be investigated with $^1$H NMR spectra which are in good agreement with the results of X-ray structural analyses. The $^1$H NMR spectra of DPASPI, hybrids **1** and **2** are represented in Fig.3. In hybrids **1** and **2**, the resonances of the two protons of the vinyl-H shift up field and the resonances of the three protons of the alkyl-H shift down field, relative to the corresponding protons of DPASPI. The results manifest that ICT is surely induced by the electron-withdrawing effects imposed by the $[Zn(NCS)_4]^{2-}$ and $[Cd(SCN)(NCS)_3]^{2-}$ anions, which indicates **1** and **2** have better photoluminescent properties than DPASPI. Interestingly, $\delta$ of 6.950 (d, $J$=8.4 Hz, 2H) and 4.251 (s, 3H) also shift to low field in **1**, in contrast to DPASPI and **2**. The FT-IR spectra (Fig.4) show characteristic band of NSC group are identified in 2 077 cm$^{-1}$.

### 2.3　Photoluminescent properties of DPASPI, hybrids 1 and 2 in solid state

It is generally acknowledged that transition metal coordination polymers assembled from Zn or Cd centers possess excellent luminescent properties, because core-like d-orbitals and thus no *d-d* transitions are possible[22]. The excitation spectra of DPASPI, hybrids **1** and **2** exhibit the wavelength band in the range of 500~600 nm, which are attributed to ICT transition of the whole molecule. The solid state emission spectra

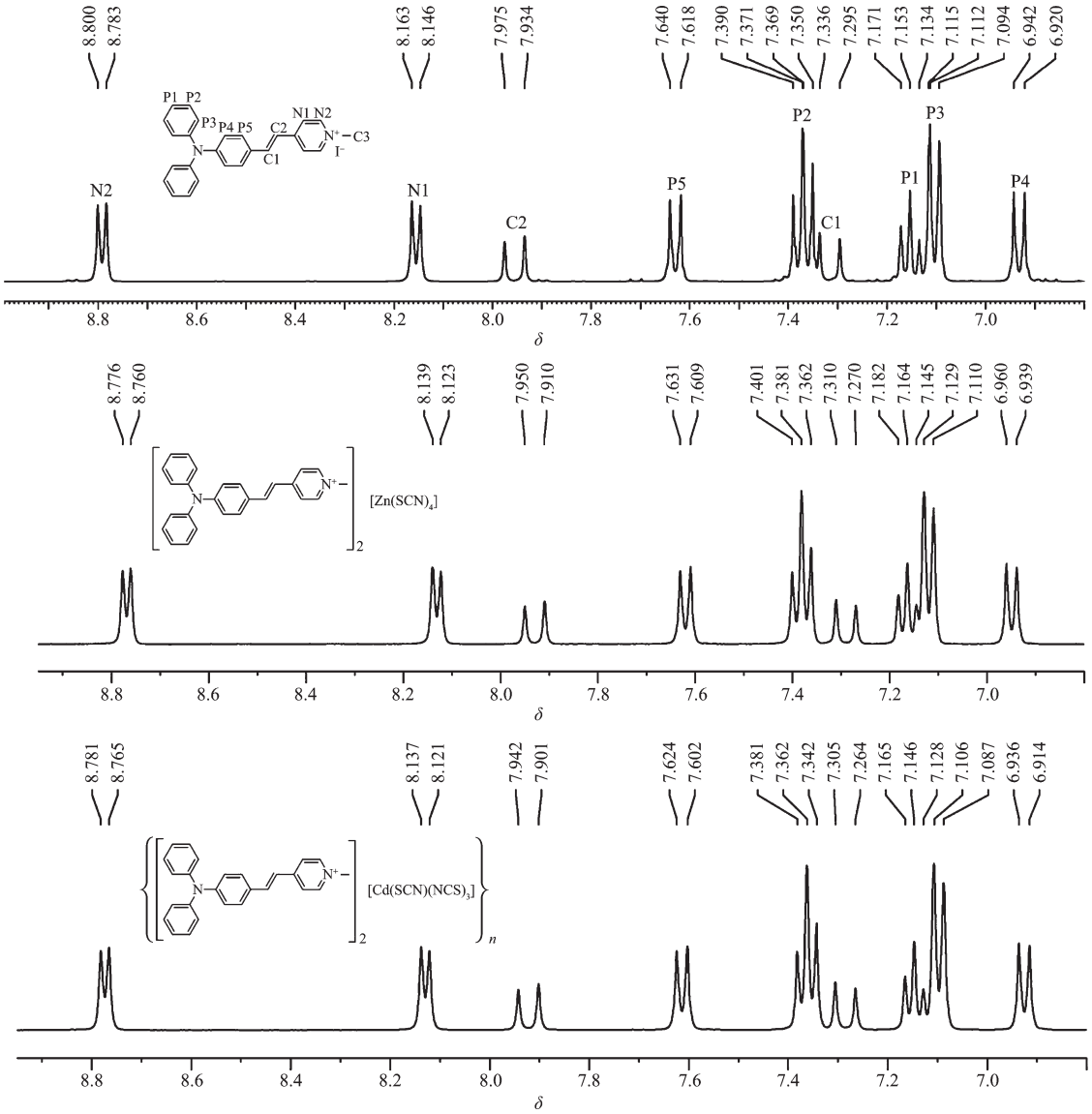


Fig.3 $^{1}$H NMR spectra of DPASPI, hybrids **1** and **2** in DMSO-$d_6$ solvent

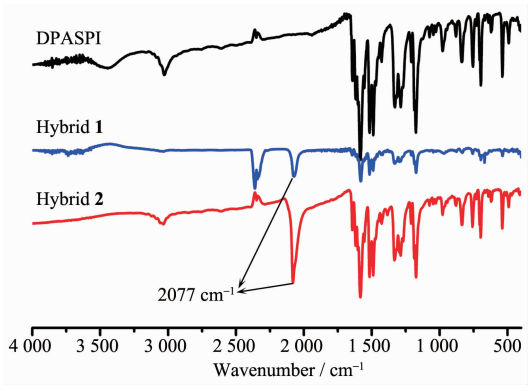


Fig.4 FT-IR spectra of DPASPI, hybrids **1** and **2**

of DPASPI, hybrids **1** and **2** have been studied at room temperature, as illustrated in Fig.5a. The emission bands at 406, 426 and 455 nm are observed for DPASPI, hybrids **1** and **2**, respectively. The different photoluminescence of hybrids **1** and **2** may be attributed to the difference in the substituting groups at $NCS^-$ and $SCN^-$ relative to the zinc/cadmium metal ions and/or their local coordination environments.

As displayed in Fig.5b, the time-resolved PL decays of DPASPI, hybrids **1** and **2** are measured using a time-correlated single-photon counting (TCSPC) technique. During the measurements, the compounds are excited with the optimal excitation wavelength ($\lambda_{ex\text{-}max}$) in order to obtain the largest relative fluorescence intensity. The fluorescence decay lifetimes and

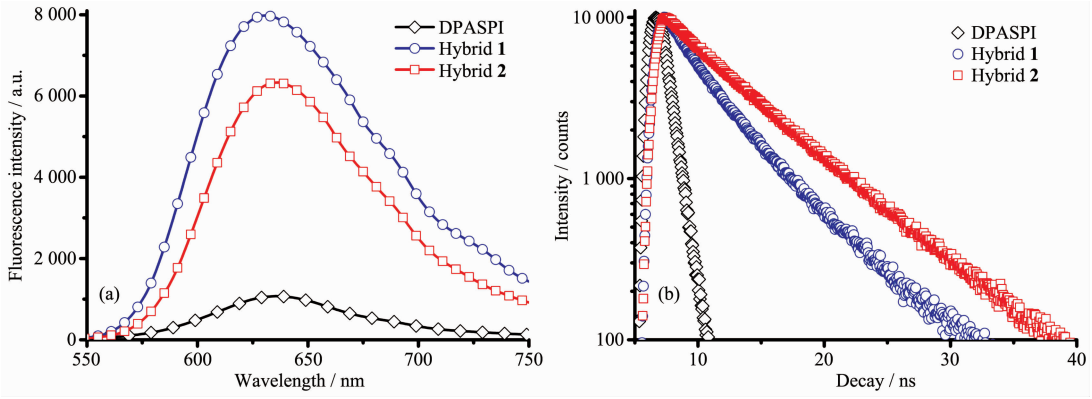


Fig.5　Emission spectra (a) and transient fluorescence (b) spectra of DPASPI, hybrids **1** and **2** in solid state at room temperature

**Table 3　$\tau$ and $\Phi_d$ of DPASPI, hybrids 1 and 2 in the solid state**

| Hybrid | $\lambda_{ex}$ / nm | $\lambda_{em}$ / nm | $\tau_1$ / ns | $A_1$ / % | $\tau_2$ / ns | $A_2$ / % | $\tau$ / ns | $\Phi$ |
|---|---|---|---|---|---|---|---|---|
| DPASPI | 458 | 535 | 7.20 | 100 | — | — | 7.20 | 0.01 |
| **1** | 386 | 631 | 3.08 | 59.76 | 7.64 | 40.24 | 4.06 | 0.19 |
| **2** | 380 | 636 | 3.66 | 20.43 | 7.23 | 79.57 | 6.03 | 0.20 |

amplitudes of DPASPI, hybrids **1** and **2** are summarized in Table 3. As previously reported[23], the result reveals that there are more than one component in the excited state of hybrids **1** and **2**. There exist two kinds of excited state, which is in accordance with the two excitation bands for hybrids **1** and **2**. However, for DPASPI there is only one excitation bands. The average fluorescence decay lifetime of **1** at 386 nm emission is 4.06 ns, and that of **2** at 380 nm is 6.03 ns. Meanwhile, the quantum yields ($\Phi$) of **1** and **2** (19% and 20%, respectively) are much larger than that of DPASPI (1%), which indicates two novel organic-inorganic hybrid multiply quantum yields approximately 20 times than DPASPI. Introducing the transition-metal thiocyanato anions to the $\pi$-conjugated pyridinium salts should provide a more stable environment for the excited state in infrared region and much enhanced fluorescence quantum yields.

Above all, hybrids **1** and **2** exhibit intense fluorescent emissions and prominent transient fluorescence in solid state at room temperature, which manifests that they have more excellent fluorescent properties than DPASPI. These emission bands (550~750 nm) in the red region suggest that these hybrids may be potential candidates as near infrared red-light-emitting materials.

## 2.4　Thermogravimetric properties

The thermogravimetry (TG) and differential thermogravimetry (DTG) curves are presented in Fig.6. The decomposition temperature (weight loss of 10 %) of DPASPI, hybrids **1** and **2** is 297, 369 and 399 ℃, respectively. At 452 ℃, DPASPI almost vanish, while

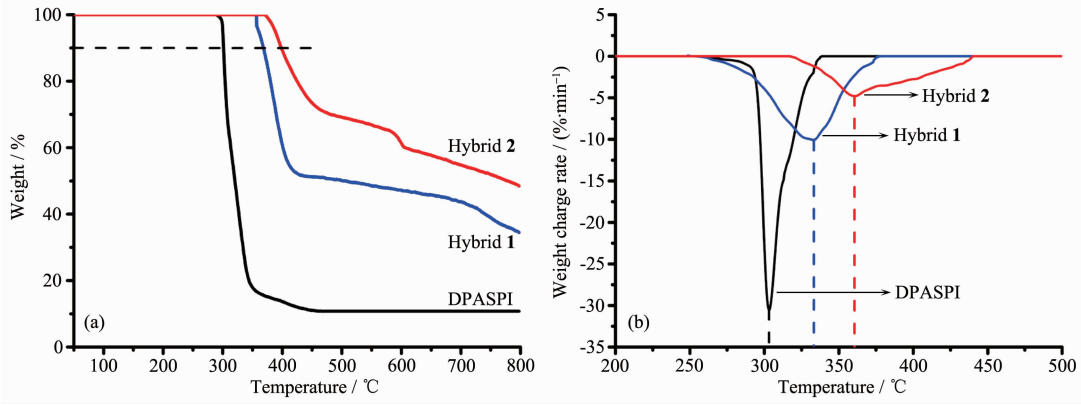


Fig.6　TG curves (a) and DTG curves (b) of DPASPI, hybrids **1** and **2**

hybrids **1** and **2** showed weight loss of about 48.7% and 27.6%, respectively. As shown in Fig.6b, $T_p$ (the maximum weight loss rate) of DPASPI, hybrids **1** and **2** is 303, 333 and 360 ℃, respectively. In short, the thermal stabilities of hybrids **1** and **2** exceed that of DPASPI largely, and hybrids **2** behaves the best.

## 3 Conclusions

In summary, we have described a facile and efficient method for the gram scale synthesis of two novel solid fluorescent organic-inorganic hybrids. Hybrids **1** and **2** have essentially different extended network structures, which have beneficial advantages for the ICT ability and photoluminescent properties. Hybrids **1** and **2** are demonstrated to display strong red fluorescence emissions in solid-state at room temperature, which suggests they might be potential near infrared-light-emitted materials. Accordingly, two hybrids bearing transition-metal thiocyanato anions, pyridinium salts turn out to be excellent fluorescent materials with enhanced quantum yield by facile replacement reaction.

## References:


[1] Nicole L, Robert C L, Rozes L, et al. *Nanoscale*, **2014**,**6**(12):6267-6292

[2] Kim H S, Pham T C T, Yoon K B. *Chem. Comm.*, **2012**,**48**(39):4659-4673

[3] Pardo R, Zayat M, Levy D. *Coord. Chem. Rev.*, **2011**,**40**(2):627-687

[4] Beverina L, Pagani G A. *Acc. Chem. Res.*, **2014**,**47**(2):319-329

[5] Langton M J, Robinson S W, Marques I, et al. *Nat. Chem.*, **2014**,**6**(12):1039-1043

[6] Therien M J. *Nat. Chem.*, **2009**,**458**(9):716-717

[7] Sullivan I, Brown C L, Llansola-Portoles M J, et al. *J. Phys. Chem. C*, **2015**,**119**(37):21294-21303

[8] Zheng Y C, Zheng M L, Li K, et al. *RSC Adv.*, **2015**,**5**(1):770-774

[9] Zhao N, Li M, Yan Y, et al. *J. Mater. Chem. C*, **2013**,**1**(31):4640-4646

[10]Xu H R, Li K, Jiao S Y, et al. *Analyst*, **2015**,**140**(12):4182-4188

[11]Dumat B, Bordeau G, Faurel-Paul E, et al. *J. Am. Chem. Soc.*, **2013**,**135**(34):12697-12706

[12]Zhao D B, Fei Z F, Geldbach T J, et al. *J. Am. Chem. Soc.*, **2004**,**126**(48):15876-15882

[13]Cole J M, Lin T C, Edwards A J, et al. *ACS Appl. Mater. Interfaces*, **2015**,**7**(8):4693-4698

[14]Ma Q, Zhu M L, Yuan C X, et al. *Cryst. Growth Des.*, **2010**,**10**(4):1706-1714

[15]Werner J, Tomkowicz Z, Reinert T, et al. *Eur. J. Inorg. Chem.*, **2015**,**15**(19):3066-3075

[16]Mahmoudi G, Morsali A. *CrystEngComm.*, **2007**,**9**(11):1062-1072

[17]Hao F Y, Zhang X J, Tian Y P, et al. *J. Mater. Chem.*, **2009**,**19**(48):9163-9169

[18]Aoyagi N, Shinha Y, Ikeda-Ohno A, et al. *Cryst. Growth Des.*, **2015**,**15**(3):1422-1429

[19]Zhao C F, He G S, Bhawalkar J aD, et al. *Chem. Mater.*, **1995**,**7**(10):1979-1983

[20]Sheldrick G M. *SHELX*-97, *Program for the Solution and the Refinement of Crystal Structures*, University of Göttingen, Germany, **1997**.

[21]Jin F, Li J F, Zhou H P, et al. *J. Mol. Struct.*, **2007**,**829**(1/2/3):202-207

[22]Niu C Y, Wu B L, Zheng X F, et al. *Cryst. Growth Des.*, **2008**,**8**(5):1566-1574

[23]Kong L, Yang J X, Zhou H P, et al. *Sci. China Chem.*, **2013**,**56**(1):106-116